Computers and Concrete, Vol. 2, No. 4 (2005) 249-266
DOI: http://dx.doi.org/10.12989/cac.2005.2.4.249

Three-dimensional FE analysis of headed stud anchors exposed to fire

Joško Ožbolt†

Institute for Construction Materials Stuttgart, University of Stuttgart, 70550 Stuttgart, Germany

Ivica Kožar‡

Faculty of Civil Engineering, University of Rijeka, 51000 Rijeka, Croatia

Rolf Eligehausen‡† and Goran Periškić‡‡

Institute for Construction Materials Stuttgart, University of Stuttgart, 70550 Stuttgart, Germany
(Received April 12, 2005, Accepted August 10, 2005)

Abstract. In the present paper a transient three-dimensional thermo-mechanical model for concrete is presented. For given boundary conditions, temperature distribution is calculated by employing a three-dimensional transient thermal finite element analysis. Thermal properties of concrete are assumed to be constant and independent of the stress-strain distribution. In the thermo-mechanical model for concrete the total strain tensor is decomposed into pure mechanical strain, free thermal strain and load induced thermal strain. The mechanical strain is calculated by using temperature dependent microplane model for concrete (Ožbolt, *et al*. 2001). The dependency of the macroscopic concrete properties (Young's modulus, tensile and compressive strengths and fracture energy) on temperature is based on the available experimental database. The stress independent free thermal strain is calculated according to the proposal of Nielsen, *et al.* (2001). The load induced thermal strain is obtained by employing the bi-parabolic model, which was recently proposed by Nielsen, *et al.* (2004). It is assumed that the total load induced thermal strain is irrecoverable, i.e., creep component is neglected. The model is implemented into a three-dimensional FE code. The performance of headed stud anchors exposed to fire was studied. Three-dimensional transient thermal FE analysis was carried out for three embedment depths and for four thermal loading histories. The results of the analysis show that the resistance of anchors can be significantly reduced if they are exposed to fire. The largest reduction of the load capacity was obtained for anchors with relatively small embedment depths. The numerical results agree well with the available experimental evidence.

Keywords: concrete; high temperature; 3D finite element analysis; microplane model; thermo-mechanical model; headed studs.

† Professor, E-mail: ozbolt@iwb.uni-stuttgart.de
‡ Professor
‡† Professor, Head of Department Fastening Technology
‡‡ Researcher

1. Introduction

Concrete does not burn, however, when its temperature increases for a couple of hundred of degrees Celsius its behavior changes significantly. The concrete mechanical properties, such as strength, elasticity modulus and fracture energy, are at high temperatures rather different than for the concrete at normal temperature. At high temperature large temperature gradients lead in concrete structures to temperature-induced stresses, which cause damage. Furthermore, creep and relaxation of concrete that is due to high temperature play also an important role. The main reason for the complexity of the behavior of concrete at high temperature is due to the fact that concrete contains water, which at high temperature changes its aggregate state. Moreover, at high temperature the aggregate can change its structure or it can loose its weight through the emission of CO_2, such as calcium based stones. Although the behaviour of concrete at high temperature is in the literature well documented (Bažant and Kaplan 1996, Khoury, *et al.* 1985a, Schneider 1986, 1988, Thelandersson 1983) further tests are needed to clarify the tensile post-peak behaviour of concrete, which has significant influence on the response of concrete structures. The main problem in the experimental investigations is due to the fact that such experiments are rather demanding, i.e., one has to perform loading and measurement at extremely high temperatures. Furthermore, such experiments can be carried out only on relatively small structures. To better understand behavior of concrete structures, as an alternative to the experiments one can employ numerical analysis. However, one needs models which can realistically predict behavior of concrete at high temperature.

There are principally two groups of models: (i) Thermo-mechanical models and (ii) Thermo-hydro-mechanical models (Gawin, *et al*. 1999, Pearce, *et al*. 2003, Stabler 2000, Terro 1998). The first group of the models are phenomenological. In these models the mechanical properties of concrete are temperature (humidity) dependent whereas the temperature (humidity) distribution is independent of the mechanical properties of concrete. The second group of the models are from the physical point of view more realistic. Namely, in these models the physical processes that take place at concrete micro structural level are coupled, i.e., the interaction between mechanical properties, temperature, humidity, pore pressure and hydration is accounted for. These models are interesting from the theoretical point of view. They are rather complex and therefore for practical engineering applications one has to employ the first group of the models.

In the present paper a three-dimensional (3D) model that is based on the thermo-mechanical coupling between mechanical properties of concrete and temperature is discussed. The isothermal microplane model is used as a constitutive law for concrete with model parameters being made temperature dependent. The model is implemented into a three-dimensional finite element code and its performance is first compared with the experimental results known from the literature. Subsequently, the influence of high temperature on the pull-out concrete cone resistance of a headed stud anchors is investigated. The finite element analysis is performed in two steps. For given temperature boundary conditions (air temperature and/or concrete surface temperature) it is first calculated distribution of temperature. In the second step the required load history is applied with taking into account the influence of temperature on the concrete mechanical properties.

2. Transient thermal analysis

As the first step of coupling between mechanical properties of concrete and temperature, for given

thermal boundary conditions at time t it has to be calculated temperature distribution over a solid structure of volume Ω. In each point of continuum, which is defined by the Cartesian coordinates (x, y, z), the conservation of energy has to be fulfilled. This can be expressed by the following equation:

$$\lambda \Delta T(x,y,z,t) + W(x,y,z,t,T) - c\rho \frac{\partial T}{\partial t}(x,y,z,t) = 0 \tag{1}$$

where T = temperature, λ = conductivity, c = heat capacity, ρ = density, W = internal source of heating and Δ = Laplace-Operator. The surface boundary condition that has to be satisfied reads:

$$\lambda \frac{\partial T}{\partial \mathbf{n}} = \alpha (T_M - T) \tag{2}$$

where $\mathbf{n}$ = normal to the boundary surface Γ, α = transfer or radiation coefficient and T_M = temperature of the media in which surface Γ of the solid Ω is exposed to (for instance temperature of air). To solve the problem by the finite element method the above differential Eqs. (1) and (2) has to be written in the weak (integral) form that reads (Belytschko, *et al.* 2001):

$$\int_\Omega \lambda \left(\frac{\partial v}{\partial x}\frac{\partial T}{\partial x} + \frac{\partial v}{\partial y}\frac{\partial T}{\partial y} + \frac{\partial v}{\partial z}\frac{\partial T}{\partial z} \right) d\Omega + \int_\Omega v \left(c\rho \frac{\partial T}{\partial t} \right) d\Omega + \int_\Gamma v\alpha (T - T_M) d\Gamma = 0 \tag{3}$$

where v is trial function. After introducing the condition that the functional is stationary one obtains the following system of linear equations (Voigt notation):

$$[C]\{\dot{T}\} + ([K] + [H])\{H\} = \{R\} \tag{4a}$$

with

$$[C] = \int_\Omega c\rho [N]^T [N] d\Omega \; ; \quad [K] = \int_\Omega [B]^T [\lambda] [B] d\Omega;$$

$$[H] = \int_\Gamma \alpha [N]^T [N] d\Gamma \; ; \quad [R] = \int_\Gamma [N]^T \alpha T_M d\Gamma \tag{4b}$$

where $[N]$ is the column matrix of shape functions that relates temperature field and nodal temperatures and $[B]$ relates the field of temperature gradients and nodal temperatures. Eq. (4a) is solved using direct method based on the following assumption for the solution in the $(n+1)^{th}$ time step

$$\{\mathbf{T}\}_{n+1} = \{\mathbf{T}\}_n + \Delta t((1-\beta)\dot{\mathbf{T}}_n + \beta \dot{\mathbf{T}}_{n+1}) \tag{5}$$

Parameter β has been set to $\beta = 0.5$ what yields to the unconditionally stable Crank-Nicolson method that reads (Cook, *et al*. 2002):

$$\left(\frac{1}{\Delta t}[C] + \beta([K] + [H]) \right) \{T\}_{n+1} = \left(\frac{1}{\Delta t}[C] - (1-\beta)([K] + [H]) \right) \{T\}_n + (1-\beta)\{R\}_n + \beta \{R\}_{n+1} \tag{6}$$

The above equation has been programmed for 3D solid finite elements.

3. Decomposition of strain

In the present model the total strain tensor ε_{ij} (indicial notation) for stressed concrete exposed to high temperature can be decomposed as (Khoury, *et al*. 1985a, Schneider 1986, Thelandersson, 1987):

$$\varepsilon_{ij} = \varepsilon^{m}_{ij}(T, \sigma_{kl}) + \varepsilon^{ft}_{ij}(T) + \varepsilon^{tm}_{ij}(T, \sigma_{kl}) + \varepsilon^{c}_{ij}(T, \sigma_{kl}) \tag{7}$$

where ε^{m}_{ij} = mechanical strain tensor, ε^{ft}_{ij} = free thermal train tensor, ε^{tm}_{ij} = thermo-mechanical strain tensor and ε^{c}_{ij} are strains that are due to the temperature dependent creep of concrete.

In general, the mechanical strain component can be decomposed into elastic, plastic and damage parts. In the present model these strain components are obtained from the constitutive law. Free thermal strain is stress independent and it is experimentally obtained by measurements on a load-free specimen. In such experiments it is not possible to isolate shrinkage of concrete. Therefore, the temperature dependent shrinkage is contained in the free thermal strain. The thermo-mechanical strain is stress and temperature dependent. It appears only during the first heating and not during the subsequent cooling and heating cycles (Khoury, *et al.* 1985a). This strain is irrecoverable and lead in concrete structures to severe tensile stresses during cooling. Temperature dependent creep stain is of the same nature as the thermo-mechanical strain except that it is partly recoverable. In an experiment it is not possible to isolate this. For low temperature rates, which is normal case in the experiments, this strain component compared to the thermo-mechanical strain is small. Therefore, temperature dependent creep stain is in the present model neglected.

4. Mechanical strain

The mechanical strain components are obtained from the constitutive law of concrete. In the present model for the temperature independent (isothermal) constitutive law the microplane model is used (Ožbolt, *et al*. 2001). The temperature dependency is adopted such that the macroscopic properties of concrete (Young's modulus, compressive and tensile strengths and fracture energy) are made time dependent.

4.1. Isothermal constitutive law for concrete – microplane model

In the microplane model the material is characterized by a relation between the stress and strain components on planes of various orientations. These planes may be imagined to represent the damaged planes or weak planes in the microstructure, such as those that exist at the contact between aggregate and the cement matrix. In the model the tensorial invariance restrictions need not be directly enforced. Superimposing in a suitable manner the responses from all the microplanes automatically satisfies them. The basic concept behind the microplane model was advanced in 1938 by Taylor and developed in detail for plasticity by Batdorf and Budianski in 1949 under the name "slip theory of plasticity". The model was later extended by Bažant and co-workers for modelling of quasi-brittle materials that exhibit softening (Bažant, *et al.* 1988, 1990, Carol, *et al*. 2001).

The microplane model used in the present study, was recently proposed by Ožbolt, *et al.* (2001). The model is based on the so-called relaxed kinematic constraint concept and it is a modification of

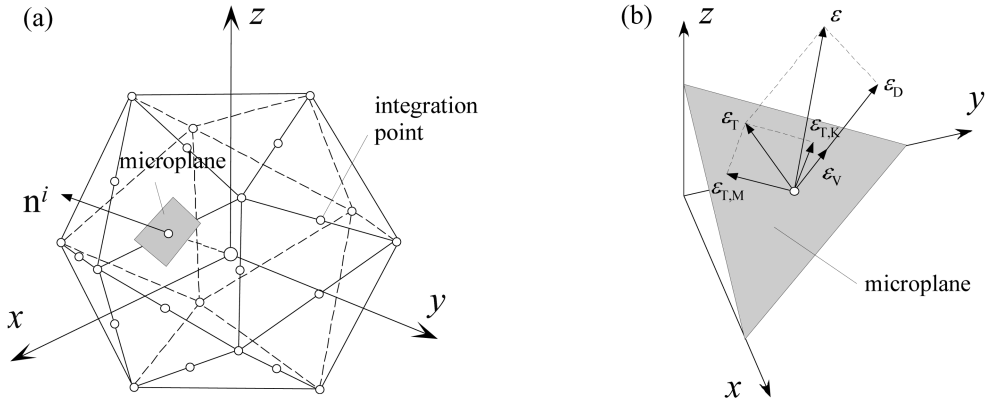

Fig. 1 The concept of the microplane model: (a) Discretization of the unit volume sphere for each finite element integration point (21 microplane directions – integration points), (b) Microplane strain components

the M2 microplane model proposed by Bažant and Prat (1988). Let ignore the effect of temperature and assume that the total strain tensor is identical to the mechanical strain tensor, i.e., $\varepsilon_{ij}^{m} = \varepsilon_{ij}$. In the model the microplane (see Fig. 1) is defined by its unit normal vector of components n_i. Microplane strains are assumed to be the projections of ε_{ij} (kinematic constraint). Normal and shear stress and strain components (σ_N, σ_{Tr}, ε_N, ε_{Tr}) are considered on each plane. Based on the virtual work approach (weak form of equilibrium), the macroscopic stress tensor is obtained as an integral over all possible, in advance defined, microplane orientations (S denotes the surface of the unit sphere):

$$\sigma_{ij} = \frac{3}{2\pi}\int_S \sigma_N n_i n_j dS + \frac{3}{2\pi}\int_S \frac{\sigma_{Tr}}{2}(n_i\delta_{rj} + n_j\delta_{rj})dS \tag{8}$$

To realistically model concrete, the normal microplane stress and strain components have to be decomposed into volumetric and deviatoric parts ($\sigma_N = \sigma_V + \sigma_D$, $\varepsilon_N = \varepsilon_V + \varepsilon_D$; see Fig. 1), which leads to the following expression for the macroscopic stress tensor:

$$\sigma_{ij} = \sigma_V\delta_{ij} + \frac{3}{2\pi}\int_S \sigma_D\left(n_i n_j - \frac{\delta_{ij}}{3}\right)dS + \frac{3}{2\pi}\int_S \frac{\sigma_{Tr}}{2}(n_i\delta_{rj} + n_j\delta_{ri})dS \tag{9}$$

For each microplane component, the uniaxial stress-strain relations read:

$$\sigma_V = F_V(\varepsilon_V); \qquad \sigma_D = F_D(\varepsilon_{D,eff}); \qquad \sigma_{Tr} = F_{Tr}(\varepsilon_{Tr,eff}, \varepsilon_V) \tag{10}$$

where F_V, F_D and F_{Tr} are the uniaxial stress-strain relationships for volumetric, deviatoric and shear components, respectively. For the deviatoric and shear microplane strain components in Eq. (10) only effective parts of microplane strains ($\varepsilon_{D,eff}$ and $\varepsilon_{Tr,eff}$), defined below, are used to calculate microplane stresses. Finally, the macroscopic stress tensor is obtained from Eq. (9). The integration over all microplane directions (21 directions, symmetric part of the sphere) is performed numerically.

To model concrete cracking for any load history realistically, the effective microplane strains are introduced in Eq. (10). They are calculated as:

$$\varepsilon_{M,eff} = \varepsilon_M \psi_M(\varepsilon_M, \sigma_I) \tag{11}$$

where subscript M denotes the corresponding microplane components (V, D, Tr), ε_M is the microplane strain obtained from the projection of the total strain tensor (kinematic constraint) and ψ is the so-called discontinuity function which depends on the microplane strain components and maximum principal stress σ_I. On the individual microplanes this function accounts for discontinuity of the macroscopic strain field (cracking). It is calculated such that for dominant tensile load the ratio between the volumetric and deviatoric stiffness remains constant for the entire load history. The function "relaxes" the kinematic constraint, which is in the case of strong localization of strains physically unrealistic. Consequently, in the smeared fracture type of the analysis the discontinuity function ψ enables localization of strains not only for tensile fracture, but also for dominant compressive type of failure. Detailed discussion of the features, development and problems related to various versions of the microplane models are beyond the scope of the present paper. For more detail refer to the above cited literature.

4.2. Thermo-mechanical coupling

To account for the effect of temperature the macroscopic mechanical properties of concrete need to be temperature dependent. The nonlinear finite element analysis is incremental and the load increment is defined by the time step Δt in which the load, the boundary conditions, the temperature, etc. change. In the present model it is assumed that during load increment the temperature is constant. Consequently, the material parameters that are temperature dependent are during the load step constant as well.

4.2.1. Young's modulus

The experiments show that with the increase of temperature Young's modulus E decreases (Thelandersson 1983). It is assumed that at relatively low temperatures decrease of E is caused by the loss of capillary water (vaporisation). However, at higher temperatures decrease of E is due to the decomposition of individual concrete components (cement paste and aggregate). In the present model, temperature dependent Young's modulus follows the proposal of Stabler (2000), i.e., E is assumed to be a scalar function of temperature that reads:

$$\begin{aligned} &E(T) = [1 - \max(\omega_{t,E})] \cdot E_0 \\ &for \quad 0 \le \theta \le 10 \qquad \omega_{t,E} = 0.2\theta - 0.01\theta^2 \\ &for \quad \theta > 10 \qquad \omega_{t,E} = 1 \end{aligned} \tag{12}$$

where E_0 = Young's modulus at temperature $T_0 = 20°C$ and $\theta = (T\text{-}T_0)/100^0C$ is the relative temperature. Eq. (12) is plotted in Fig. 2. As can be seen, it shows good agreement with the experimental evidence. Note that $\max(\omega_{t,E})$ corresponds to the maximal temperature ever reached, i.e., by cooling Young's modulus does not increases.

4.2.2. Compressive strength of concrete

According to the experimental evidence (Abrams 1971, Schneider 1986, Zhang and Bićanić, 2002), for temperatures up to 300°C the concrete compressive strength slightly increases with increase of temperature. However, with further increase of temperature, the concrete strength

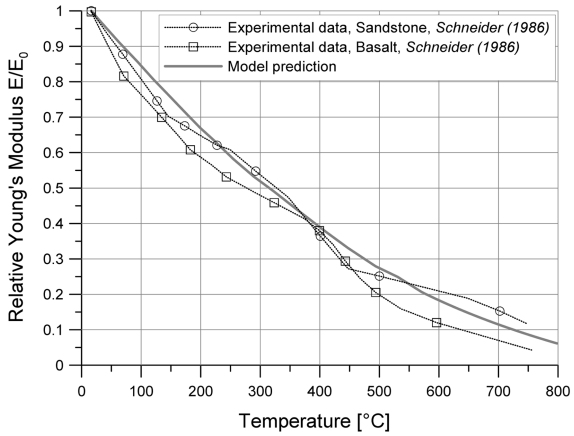

Fig. 2 Relationship between the Young's modulus and temperature

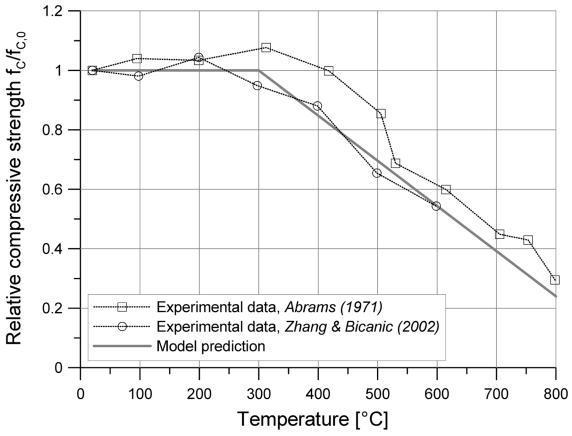

Fig. 3 Relationship between the concrete compressive strength and temperature

decreases almost linearly. Namely, at lower temperatures hydration of cement paste is more advanced. Moreover, due to the thermal strains the frictional and aggregate locking phenomena are even stronger than for the concrete at normal temperature. Due to these effects the compressive strength does not decrease. At extremely high temperature, microcracks, vaporisation and decomposition of cement paste and aggregate cause decrease of the concrete compressive strength. In the present model it is assumed that up to $T = 300°C$ the cylinder compressive strength f_c is temperature independent and for higher temperature it decreases as a linear function of temperature:

$$\begin{aligned} &E(T) = \max(\omega_{t,E}) f_{c,0} \\ &for \;\; 0 \le \theta \le 2.80, \quad \omega_{t,f_c} = 1.0 \\ &for \;\; \theta > 2.80, \quad \omega_{t,f_c} = 1.43 - 0.153\,\theta \end{aligned} \tag{13}$$

where $f_{c,0}$ = uniaxial compressive strength at $T = 20°C$. The adopted dependency is plotted in Fig. 3 and compared with experimental results. As can be seen the comparison shows good agreement.

4.2.3. Tensile strength of concrete

The experimental evidence indicates that the tensile strength of concrete decreases almost linearly with increase of temperature (Schneider 1986, Zhang and Bićanić, 2002). At lower temperatures thermal strains lead to micro cracking and damage of the aggregate-cement paste interface which reduces tensile strength of concrete. With increase of temperature, micro-cracks, vaporisation and decomposition of cement paste and aggregate also lead to further decrease of the concrete tensile strength. In the present model the following dependency of tensile strength on temperature is adopted:

$$f_t(T) = \max(\omega_{t,f_t}) f_{t,0}, \qquad \omega_{t,f_t} = 1 - 0.131\,\theta \tag{14}$$

where $f_{t,0}$ = uniaxial compressive strength at $T = 20°C$. The plot of Eq. (14) is shown and compared with the test data in Fig. 4.

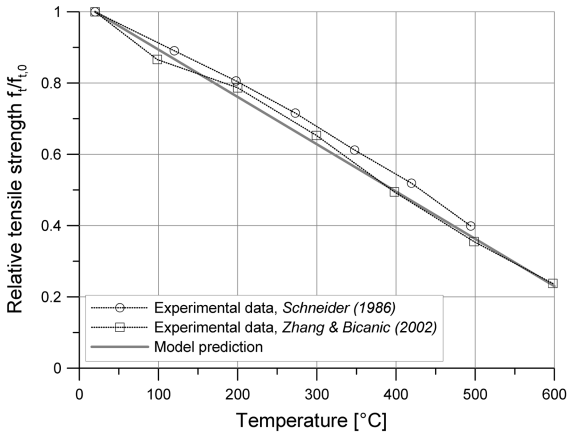

Fig. 4 The relative tensile strength as a function of temperature

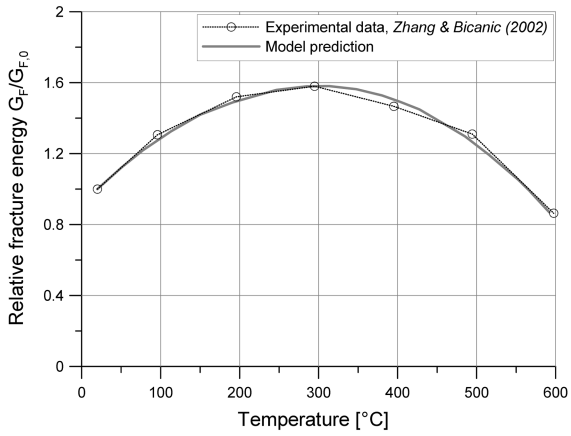

Fig. 5 The relative concrete fracture energy as a function of temperature

4.2.4. Fracture energy of concrete

A recent experimental investigation (Zhang and Bićanić 2002) show that with the increase of temperature up to approximately 300°C the concrete fracture energy increases for approximately 60%. However, with further increase of temperature it starts to decrease and at approximately 600°C reaches about 90% of its initial value. This can be explained by the fact that at temperatures between approximately 100 and 300°C, the degree of hydration is higher than at normal room temperature. Moreover, at this stage temperature strains contribute to the frictional effects and aggregate interlock, which increases ductility. At higher temperatures the microcracks, vaporisation and decomposition of cement paste and aggregate cause decrease of concrete ductility. In the present model, the dependency of the concrete fracture energy G_F on the temperature is obtained by fitting of the test data by Zhang and Bićanić (2002). The adopted dependency reads:

$$
\begin{aligned}
& G_F(T) = \max(\omega_{t,G_F}) G_{F,0} \\
& for \;\; 0 \le \theta \le 2.80, \qquad \omega_{t,G_F} = 1 + 0.407\theta - 0.0727\theta^2 \\
& for \;\; \theta > 2.80, \qquad \omega_{t,G_F} = 0.917 + 0.4670\theta - 0.0833\theta^2
\end{aligned}
\tag{15}
$$

where $G_{F,0}$ = concrete fracture energy at $T = 20$°C. Eq. (15) is plotted in Fig. 5 and compared with experimental results. As can be seen, the comparison shows good agreement.

5. Thermal strain

As mentioned before, the total thermal strain generated as a consequence of heating of concrete can be decomposed into strains that are stress independent (free thermal strains) and strains, which are stress dependant (stress induced thermal strains).

5.1. Free thermal strain

The experimental evidence (Schneider 1986) indicates that free thermal strains in concrete specimen mainly depend on the type and amount of the aggregate. As can be seen from Fig. 6, the relationship between the free thermal strain and temperature is highly non-linear and dependent on the thermal stability of the aggregate. Although the experiments indicate that the free thermal strain depends on the rate of temperature, in the present model is assumed that this strain depends only on the temperature. Moreover, it is assumed that in the case of a stress free specimen, thermal strains in all three mutually perpendicular directions are the same (isotropic thermal strains). In the present model the rate of the free thermal strain is calculated as (indicial notation) (Nielsen, *et al*. 2001):

$$\begin{aligned} &\dot{\varepsilon}_{ij}^{ft} = \alpha \dot{T} \delta_{ij} \\ &for \quad 0 \le \theta \le 6, \qquad \alpha = \frac{6.0 \times 10^{-5}}{7 - \theta} \\ &for \quad \theta > 6, \qquad \alpha = 0 \end{aligned} \tag{16}$$

where δ_{ij} is Kronecker delta. The above equation is plotted in Fig. 6. In the same figure are also shown the experimental results for concrete made of three different aggregate types (Schneider, 1986). It can be seen that the free thermal strain very much depends on the aggregate tape. Up to approximately 600°C the free thermal strain increases with increase of temperature, however, further increase of temperature causes no further increase of thermal strain. The reason for this is that beyond 600°C the change of the crystalline structure of the aggregate takes place (Bažant and Kaplan 1996). The relationship (16) is chosen such that only the main trend is covered but not the exact development of free thermal strains for particular concrete type.

5.2. Stress induced thermal strain – creep

When a concrete specimen is first loaded and than exposed to high temperature, the resulting thermal strain is different from the one when the specimen is not loaded (Bažant and Chern 1987, Khoury, *et al*. 1985b, Thelandersson 1987, Thienel 1993, Thienel and Rostassy 1996). The difference can be obtained if the free thermal strain is subtracted from the resulting thermal strain. This difference is in the literature known as stress induced thermal strain. As already mentioned, the stress induced thermal strain consists of two parts – irrecoverable part and partly recoverable part (temperature dependent creep). Since the partly recoverable part has only theoretical meaning and is much smaller than the irrecoverable part, in the present model it is neglected, i.e., the total stress dependent thermal strain is assumed to be irrecoverable.

Based on the experimental evidence, in the present model the bi-parabolic thermo-mechanical strain model is used (Nielsen, *et al*. 2004). The uniaxial (scalar) rate form of this model reads:

$$\begin{aligned} &\dot{\varepsilon}^{tm}(T,\sigma) = \frac{\sigma}{f_c^{T_0}} \beta \dot{T} \\ &\beta = 0.01 \cdot \begin{Bmatrix} 2 \cdot A \cdot \theta + B & for \quad 0 \le \theta \le \theta^* = 4.5 \\ 2 \cdot C \cdot (\theta - \theta^*) + 2 \cdot A \cdot \theta^* + B & for \quad \theta > \theta \end{Bmatrix} \end{aligned} \tag{17}$$

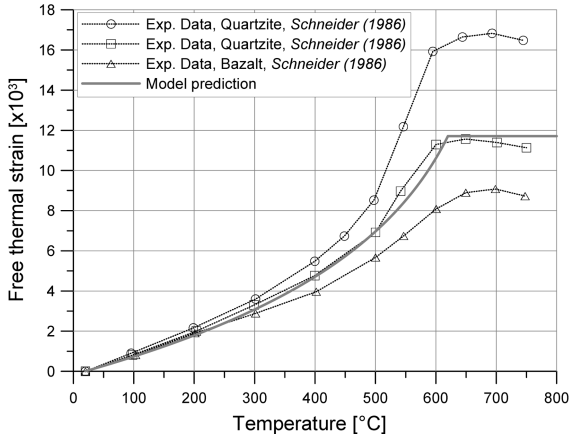

Fig. 6 The relationship between temperature and free thermal strain – adopted curve and test data for concrete with three different aggregate types (Schneider, 1986)

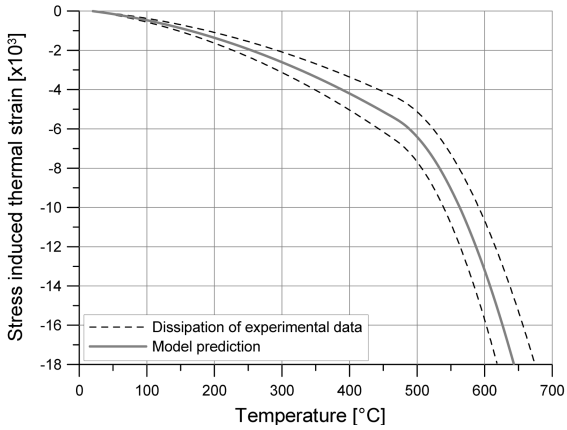

Fig. 7 Stress induced thermal strain as a function of temperature (Schneider 1986)

where θ^* is a dimensionless transition temperature between the two expressions which correspond to 470°C. The above two expressions are introduced to account for abrupt change in behavior detected in the experiments. A, B and C are experimentally obtained constants that are in the present model set as: $A = 0.0005$, $B = 0.00125$ and $C = 0.0085$.

All experimental investigations for stress induced thermal strain are performed for sustained compressive load and there is no test available for sustained tensile load. Because of this and the fact that the tensile stress is limited by the relative small tensile strength of concrete, it is assumed that Eq. (17) applies only on compressive stress. Furthermore, it is assumed that the Poisson's ratio, which relates axial and lateral stress induced thermal strains, is a material constant equal to the Poisson's ratio of undamaged concrete. Based on these assumptions the three-dimensional form of Eq. (17) reads:

$$\dot{\varepsilon}_{ij}^{tm}(T,\sigma_{ij}) = \frac{\beta}{f_c^{T_0}}((1+\nu)\bar{\sigma}_{ij} - \nu\bar{\sigma}_{kk}\delta_{ij})\dot{T}(T_{\max})$$
$$\dot{T}(T_{\max}) = \dot{T} \quad for \quad T \geq T_{\max}; \dot{T}(T_{max}) = 0 \quad for \quad T < T_{\max} \tag{18}$$

where '–' indicates compressive stress, i.e. tensile stress components of the stress tensor are set to zero. $T_{\max}$ is the maximal temperature reached so far and it is introduced in Eq. (18) to recognize the irreversible nature of thermo-mechanical strain.

6. Numerical studies

The presented thermo-mechanical model for concrete is implemented into a 3D finite element (FE) code. The implementation is first verified on two examples from the literature. Subsequently, the influence of the high temperature on the performance of a headed stud anchor that is pulled out from a concrete block is studied.

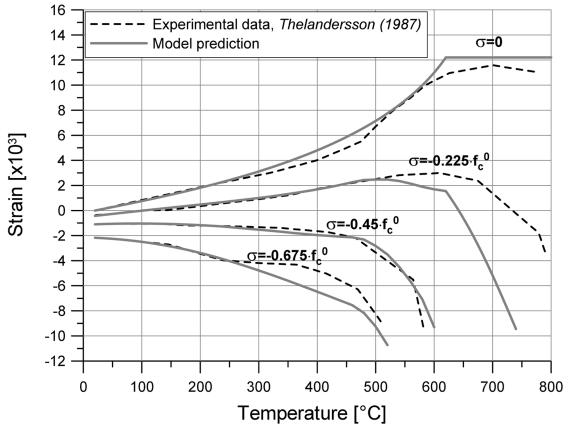

Fig. 8 Total strains versus temperature

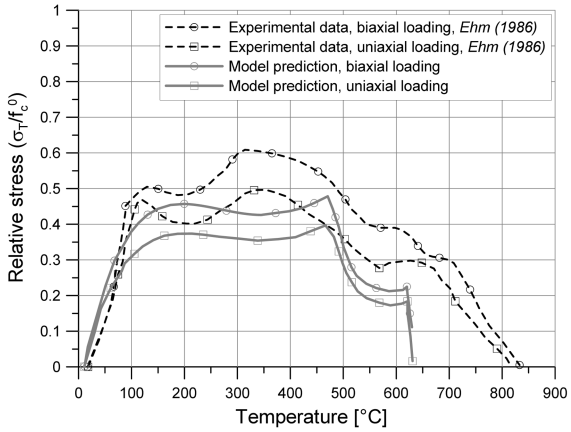

Fig. 9 Thermal induced stresses versus temperature

6.1. Verification

In the first example, transient test data reported by Thelandersson (1987) are reproduced using the presented model. The concrete cylinder was loaded by different levels of sustained compressive loads and heated by constant heating rate. The specimen geometry (cylinder) was discretized by eight node solid finite elements. The results of the numerical analysis are shown in Fig. 8. As can be seen, the numerical prediction fits the experimental data for all load histories very well.

In the second example a concrete specimen with in-plane fully restrained ends and with only two restrained ends, respectively, were exposed to the constant heating rate (Ehm 1986). The numerical analysis for both boundary conditions was performed by the use of the eight node solid finite elements. The results of the analysis are shown in Fig. 9. The comparison between numerical and experimental results shows again good trend.

6.2. Pull-out of headed stud anchor from a concrete block

The performance of a headed stud anchors exposed to high temperature is numerically investigated. A concrete block with a single headed anchor (see Fig. 10) was exposed to fire at its upper side (anchor side). The analysis consists of two parts. In the first part a 3D transient thermal FE analysis was carried out. The resulting thermal distribution is then used in the second part of the analysis in which the above presented thermo-mechanical model was applied.

The investigated geometry was principally the same as the one tested by Reick (2001). However, in the experiment the concrete block was relatively large. To save computer time, a concrete member of a diameter $d_S = 370$ mm and thickness $t = 160$ mm was used for the analysis of anchors with embedment depths $h_{ef} = 25$ and 50 mm. For anchors with $h_{ef} = 150$ mm the dimensions of the concrete member were take as $d_S = 2180$ mm and $t = 550$ mm (see Fig. 10a). The typical finite element mesh, in which a four node solid elements were used, is shown in Fig. 10b. One fourth of the geometry was discretized, i.e., double symmetry was utilized. To approximately meet experimental boundary conditions, two outer vertical rows of the finite elements around the concrete block were taken as linear elastic. The upper (heated) side of the specimen was supported in vertical direction.

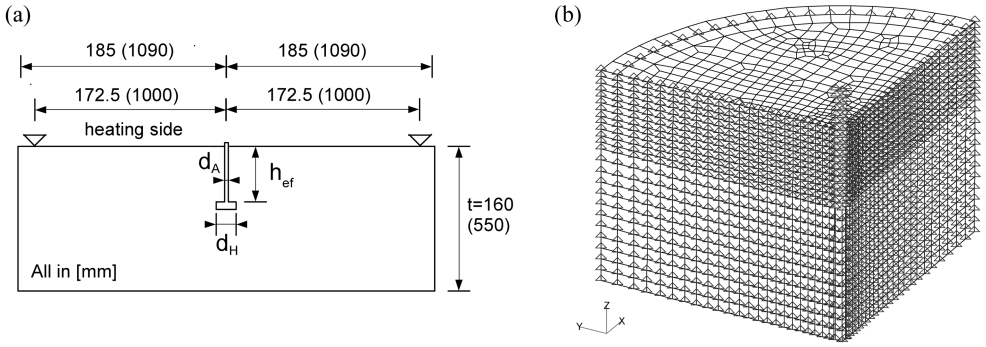

Fig. 10 Pull-out of the headed stud anchor from a concrete block: (a) Geometry of the specimen, (b) Typical finite element discretization of the concrete specimen

Table 1 Mechanical and thermal properties of steel and concrete used in the FE analysis.

	Concrete	Steel
Young's modulus E [MPa]	28000	200000
Poisson's ratio ν	0.18	0.34
Tensile strength f_t [MPa]	2.5	
Uniaxial compressive strength f_c [MPa]	21.25	
Fracture energy G_F [Nmm/mm^2]	0.07	
Conductivity λ [W/(mK)]	2.0	53.0
Heat capacity c [J/(kgK)]	900	470
Density ρ [kg/m^3]	2300	7850
Transfer coefficient α [W/(m^{2}K)]	8.0	99.0

The diameter of the supporting ring was 345 (2000) mm. The thermal and mechanical properties of concrete used in the analyses are summarized in Table 1. To prevent anchor failure, the behaviour of steel is assumed to be linear elastic.

The FE analysis was carried out for three different embedment depths $h_{ef} = 25$ mm ($d_A = 8$ mm and $d_H = 13$ mm - see Fig. 10a), $h_{ef} = 50$ mm ($d_A = 10$ mm and $d_H = 20$ mm) and $h_{ef} = 150$ mm ($d_A = 10$ mm and $d_H = 26$ mm). For all analysed embedment depths, anchor was first pre-loaded by design load at temperature of $T = 20$°C ($h_{ef} = 25$ mm, $P_D = 1.5$ kN; $h_{ef} = 50$ mm, $P_D = 5.7$ kN; $h_{ef} = 150$ mm, $P_D = 30.0$ kN). In the next step the fire was applied at the anchor side of the specimen. The air heating temperature at the upper specimen side was taken according to ISO 833 (equivalent to DIN 4102, part 2):

$$T_{Air}(t) - T_{Air}(t_0) = 345 log(8t + 1) \tag{19}$$

where $T_{Air}(t_0)$ is the air starting temperature (in our case room temperature of 20°C) and t is time in minutes measured from the start of the fire. In the case of cooling, it was assumed that the air temperature is linearly decreasing from the start of cooling back to the room temperature of 20°C (see Fig. 11a). The temperature at the bottom side of the specimen was assumed to be constant during the entire thermal loading history and equal to 20°C.

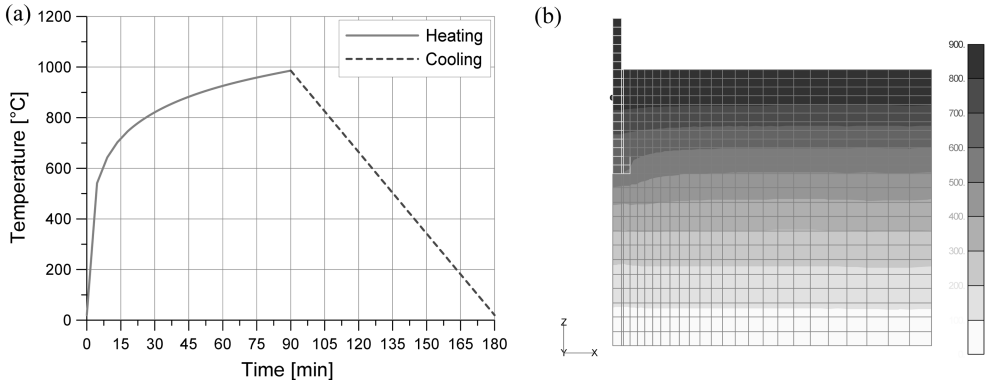

Fig. 11 Thermal loading: (a) Assumed temperature increase of air as a function of time, (b) Calculated temperature distribution in °C after $t = 90$ min

Fig. 11 b shows distribution of temperature in the concrete specimen ($h_{ef} = 50$ mm), 90 minutes after start of fire. As one would expect, due to the relatively high conductivity of steel, temperature of concrete around the anchor is higher than in the rest of the specimen. The numerical analysis shows that after cooling of the upper concrete surface down to the room temperature (180 minutes after start of fire), in the mid of the concrete specimen the temperature was still around 300°C.

To investigate the pull-out resistance, the anchor was pulled out from a concrete block for the following thermal loading histories: (i) before heating, (ii) 30 minutes after start of heating, (iii) 90 minutes after start of heating and (iv) after 90 minutes of heating followed by 90 minutes of cooling back to the air temperature of 20°C. Calculated load-displacement curves for $h_{ef} = 25$ and 150 mm and for four thermal loading histories are plotted in Fig. 12. The relative resistance is calculated as the ratio of the calculated temperature dependent resistance to the calculated pull-out resistance of unheated concrete. Fig. 13 shows the relative anchor resistance as a function of embedment depth (Fig. 13a) and the relative anchor resistance as a function of time (Fig. 13b) for all three embedment depths and for all thermal loading histories. For the third loading history, Fig. 13a shows the available test data (Reick 2001). It can be seen that the numerical results fit well the experimental results.

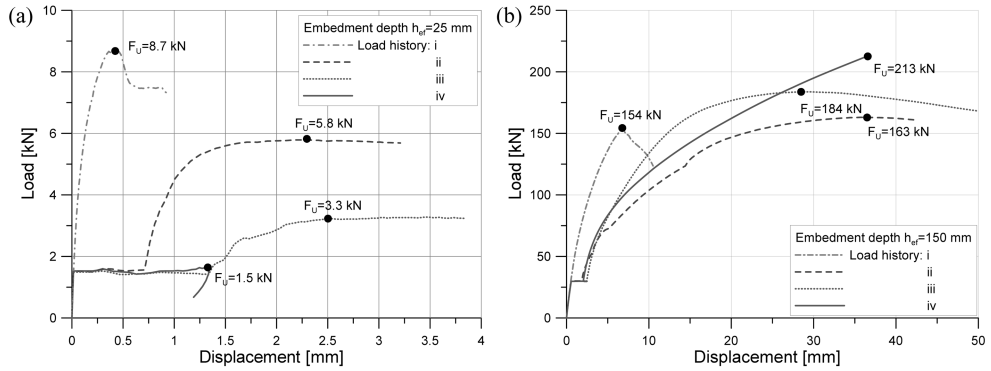

Fig. 12 Typical calculated load-displacement curves for all four thermal loading histories with embedment depths: (a) $h_{ef} = 25$ mm, (b) $h_{ef} = 150$ mm (solid dots indicate maximum load)

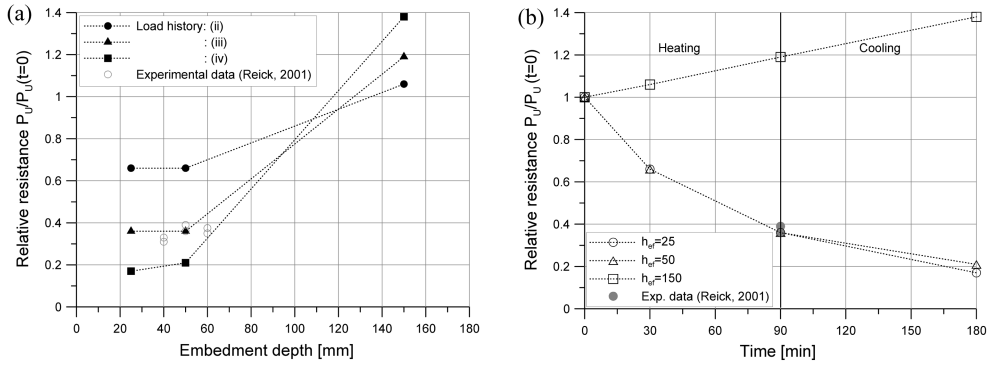

Fig. 13 Relative pull-out resistance: (a) A function of embedment depth, (b) a function of temperature

As expected, due to damage caused by thermal loading, the pull-out resistance of a headed stud anchors is significantly reduced. It can be seen that with increase of temperature the peak load and stiffness of anchors decrease. Moreover, displacement at peak load significantly increases if the concrete member was exposed to fire. Compared to the initial resistance at $t = 0$ and $T_{Air} = 20°C$, the largest reduction of the ultimate load was obtained for the smallest embedment depth ($h_{ef} = 25$ mm) and for the forth thermal loading history (90 min. heating followed by 90 min. cooling). However, this does not hold for all embedment depths. The pull-out behaviour of anchors with $h_{ef} = 150$ mm shows somewhat different response from the one for anchors with smaller embedment depth. Namely, for the second and third thermal loading history there is no reduction of the pull-out capacity. Moreover, for cooling the pull-out resistance is even greater than the pull-out resistance at room temperature.

For relatively small embedment depths the anchor lies over the entire length in the zone of very high temperature in which the concrete is almost completely destroyed. Extreme cases are observed for embedment depths $h_{ef} = 25$ and 50 mm and for the forth loading history. For these cases the ultimate pull-out capacity is even smaller than the initially applied design load (see Figs. 12a), i.e., the anchors failed during cooling. The reason is the existence of large thermal strains, which are partly irreversible, and which in restrained concrete member generate tensile stresses and damage. This damage, together with the degradation of concrete mechanical properties at high temperature, causes significant reduction of the pull-out resistance. To illustrate the effect of the thermal strains, Fig. 14a shows damage (dark zones) of the concrete block with $h_{ef} = 25$ mm, which was heated and than cooled down according to the forth thermal loading history, through the maximal principal strains of the mechanical strain tensor. The vertical cracks in concrete, which appear as a consequence of cooling, can be clearly recognized.

For larger anchors and especially if the embedment depth is large compared to the thickness of a concrete member, the head of the stud lies in the zone of lower temperature. In this zone the concrete is less damaged. Moreover, due to the restraining conditions it is possible that the head of the anchor comes into the zone in which the stresses perpendicular to the axis of the anchor are compressive. Such conditions contribute to the relatively low reduction of the pull-out resistance or, as in the present case, to an increase of it. To illustrate this, Fig. 14b shows distribution of horizontal stresses (σ_{yy}) for the embedment depth of 150 mm after cooling of the concrete member ($t = 190$ min). As can be seen, the head of the stud comes into the compressive zone. This explains

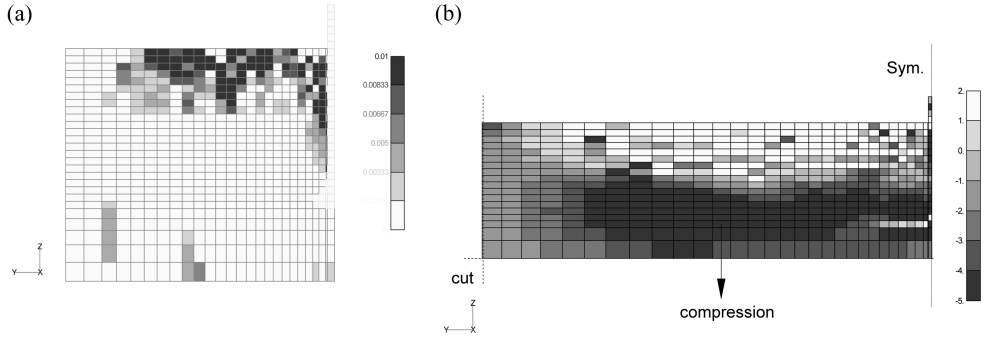

Fig. 14 Results of the thermal analysis: (a) Damaged zone in the concrete member (h_{ef} = 50 mm) after heating and cooling – maximal principal strains of the mechanical strain tensor, (b) Distribution of horizontal stresses σ_{yy} after heating and cooling (h_{ef} = 150 mm)

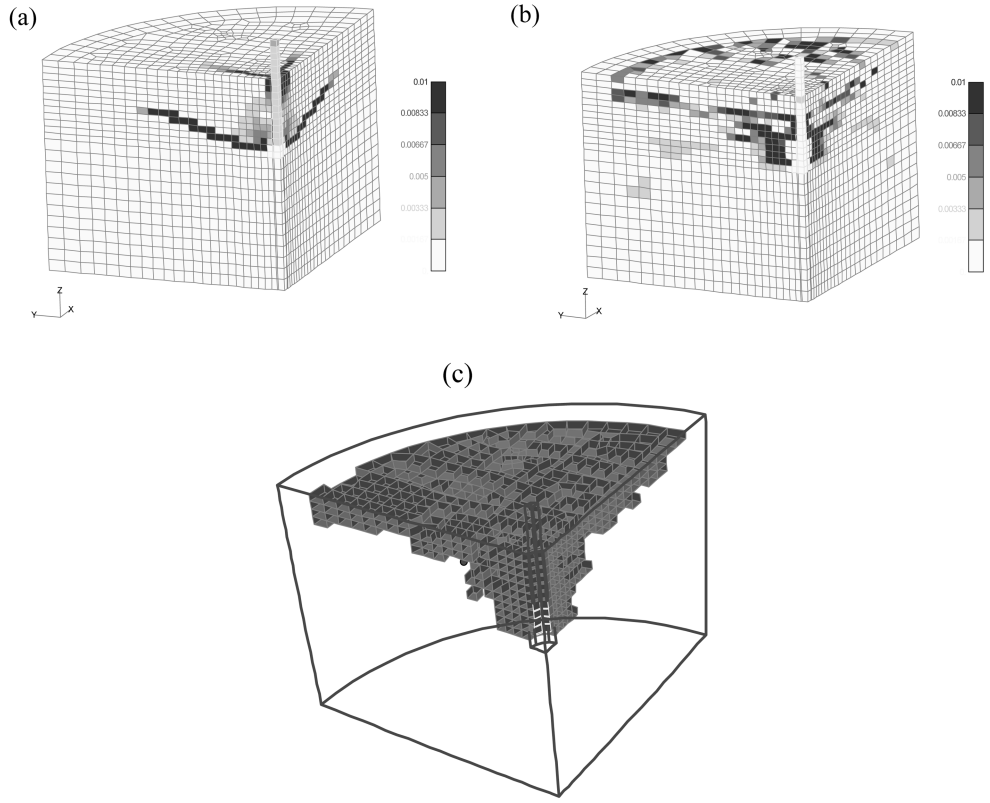

Fig. 15 Typical crack patterns for h_{ef} = 50 mm: (a) Unheated specimen, (b) Specimen exposed 90 min. to fire (loading history (iii)), (c) The concrete cone for the case shown in (b)

why the resistance of the anchor in case of the fourth loading history becomes large than the resistance of the anchor pulled out from unheated concrete member.

Fig. 15a shows a typical crack pattern (maximal principal strains of the mechanical strain tensor)

for unheated concrete member (h_{ef} = 50 mm). Fig. 15b shows a typical crack pattern for the anchor (h_{ef} = 50 mm) pulled out from heated concrete member (third thermal loading history). As can be seen, for unheated specimen a typical concrete cone forms. The crack starts from the head of the stud and propagates under an average angle of 35° to the horizontal plane. On the contrary to this, for the heated specimen the angle of the crack propagation close to the anchor head is rather steep. As it approaches the surface of the concrete member, where the concrete is completely destroyed, the crack becomes almost horizontal. Typical failure cone is shown in Figure 15c. This observation is in a very good agreement with experimental evidence.

7. Conclusions

In the present paper a transient three-dimensional thermo-mechanical model for concrete is presented. For a given boundary conditions, temperature distribution is calculated by the three-dimensional transient thermal finite element analysis using direct integration method. The thermal properties of concrete are assumed to be constant and independent of the stress-strain distribution. In the thermo-mechanical model the total strain is decomposed into pure mechanical strain, free thermal strain and load induced thermal strain. The mechanical strain is calculated based on the temperature dependent microplane model for concrete (Ožbolt, *et al*. 2001). The dependency of the macroscopic concrete properties (Young's modulus, tensile & compressive strength and fracture energy) on temperature is taken from the available experimental database. The free thermal strain, which is stress independent, is calculated by following the proposal of Nielsen, *et al*. (2001). The bi-parabolic model proposed by Nielsen, *et al*. (2004) is used for the prediction of the load induced thermal strain. It is assumed that the total load induced thermal strain is irrecoverable, i.e., creep component is neglected. The model is implemented into a three-dimensional FE code.

To check the model and its implementation two examples taken from the literature were analyzed. In the first the load independent strain and the load dependent thermal strain were predicted. In the second example the thermal induced stresses were calculated. In both cases the model prediction agrees well with the experimental data. Subsequently, the performance of headed stud anchors under fire was investigated. For a given geometry of the concrete member with a constant concrete properties, three-dimensional transient thermal FE analysis was carried out for three embedment depths and for four thermal loading histories. The analysis shows that the resistance of anchors with relatively small embedment depth can be significantly reduced if they are exposed to fire. This is especially true if the concrete member is first exposed to fire and than cooled down. In such a case for small embedment depth the anchor resistance is even smaller than design load. These results agree well with the experiments. For $h_{ef} \geq 150$ mm a slight increase of the pull-out resistance was obtained.

Further studies are needed to investigate the pull-out problem in more detail. Finally, it can be concluded that the presented, relatively simple, model is a powerful numerical tool which can be used to clarify the behavior of a number of structures and structural components exposed to fire.

References

Abrams, M. S. (1971), "Compressive strength of concrete at temperatures to 1600F", *ACI SP 25, Temperature and Concrete*, American Concrete Institute, Detroit.

Batdorf, S. B. and Budianski, B. (1949), "A mathematical theory of plasticity based on the concept of slip", *Technical Note No. 1871*, National Advisory Committee for Aeronautics, Washington D.C.

Bažant, Z. P. and Chern, J. C. (1987), "Stress-induced thermal and shrinkage strains in concrete", *J. Eng. Mech.*, **113**(10), 1493-1511.

Bažant, Z. P. and Prat, P. C. (1988), "Microplane model for brittle-plastic material - Parts I and II", *J. Eng. Mech.,* **114**(10), 1672-1702.

Bažant, Z. P. and Ožbolt, J. (1990), "Nonlocal microplane model for fracture, damage and size effect in structures", *J. of Eng. Mech.*, **116**(11), 2485-2504.

Bažant, Z. P. and Kaplan, M. F. (1996), *Concrete at High Temperatures: Material Properties and Mathematical Models*, Harlow, Longman.

Carol, I., Jirásek, M. and Bažant, Z. P. (2001), "New thermodynamically consistent approach to microplane theory: Part I - Free energy and consistent microplane stress", *Int. J. Solid. and Struct.*, **38**(17), 2921-2931.

Belytschko, T., Liu, W. K. and Moran, B. (2001), *Nonlinear Finite Elements for Continua and Structures,* John Wiley & Sons Ltd.

Cook, R. D., Malkus, D. S., Plesha, M. E. and Witt, R. J. (2002), *Concepts and Applications of Finite Element Analysis*, 4th edition, John Wiley & Sons Inc.

Ehm, C. (1986), "Versuche zur Festigkeit und Verformung von Beton unter zweiaxialer Beanspruchung und hohen Temperaturen", PhD thesis, Heft 71, TU Braunschweig, Braunschweig.

Gawin, D., Majorana, C. E. and Schrefler, B. A. (1999), "Numerical analisys of hygro-thermal behaviour and damage of concrete at high temperatures", *Mech. Cohes.-Frict. Mater.*, **4**(1), 37-74.

Khoury, G. A.,Grainger, B. N. and Sullivan, P. J. E. (1985a), "Transient thermal strain of concrete: literature review, conditions within specimens and behaviour of individual constituents", *Mag. of Conc. Res.*, **37**(132), 131-144.

Khoury, G. A., Grainger, B. N. and Sullivan, P. J. E. (1985b), "Strain of concrete during first heating to 600°C under load", *Mag. of Conc. Res.*, **37**(133), 195-215.

Nielsen, C. V., Pearce, C. J. and Bićanić, N. (2001), "Theoretical model of high temperature effects on uniaxial concrete member under elastic restraint", *Mag. of Conc. Res.*, **54**(4), 239-249

Nielsen, C. V., Pearce, C. J. and Bićanić, N. (2004), "Improved phenomenological modelling of transient thermal strains for concrete at high temperatures", *Comput. and Conc.,* **1**(2), 189-209.

Ožbolt, J., Li, Y.-J. and Kožar, I. (2001), "Microplane model for concrete with relaxed kinematic constraint", *Int. J. Solid. and Struct.*, **38(**16), 2683-2711.

Pearce, C. J., Bićanić, N. and Nielsen, C. V. (2003), "A transient thermal creep model for concrete", *Computational Modeling of Concrete Structures,* Sweets & Zeitlinger, Lisse.

Reick, M. (2001), "Brandverhalten von Befestigungen mit großem Randabstand in Beton bei zentrischer Zugbeanspruchung", *Mitteilungen des Institut für Werkstoffe im Bauwesen*, Band 2001/4, IWB, Universität Stuttgart, Stuttgart.

Schneider, U. (1986), *Properties of Materials at High Temperatures, Concrete*, 2nd. Edition, RILEM Technical Comitee 44-PHT, Technical University of Kassel, Kassel.

Schneider, U. (1988), "Concrete at high temperatures – A general review", *Fire Safety J.,* **13**(1), 55-68

Stabler, J. (2000), "Computational modelling of thermomechanical damage and plasticity in concrete", PhD thesis, The University of Queensland, Brisbane.

Taylor, G. I. (1938), "Plastic strain in metals", *J. of the Inst. of Metals.*, **62**, 307-324.

Terro, M. J. (1998), "Numerical modelling of the behaviour of concrete structures in fire", *ACI Struct. J.*, **95**(2), 183-193.

Thelandersson, S. (1983), "On the multiaxial behaviour of concrete exposed to high temperature", *Nucl. Eng. and Design*, **75**(2), 271-282.

Thelandersson, S. (1987), "Modelling of combined thermal and mechanical action in concrete", *J. Eng. Mech.*, **113**(6), 893-906.

Thienel, K.-C. (1993), "Festigkeit und Verformung von Beton bei hoher Temperatur und biaxialer Beanspruchung – Versuche und Modellbildung", PhD thesis, Heft 10, IBMB, TU Braunschweig, Braunschweig.
Thienel, K.-C. and Rostassy, F. S. (1996), "Transient creep of concrete under biaxial stress and high temperature", *Cem. and Conc. Res.*, **26**(9), 1409-1422.
Zhang, B. and Bićanić, N. (2002), "Residual fracture toughness of normal- and high-strength gravel concrete after heating to 600°C", *ACI Mater. J.,* **99**(3), 217-226.

CC